Study of the Core−Shell Nanoparticle Formed through the "Coil-to-Globule" Transition of Poly(*N*-isopropylacrylamide) Grafted with Poly(ethylene oxide)

Xingping Qiu and Chi Wu*

Department of Chemistry, The Chinese University of Hong Kong, Shatin N.T., Hong Kong, China

Received June 19, 1997; Revised Manuscript Received September 30, 1997[⊗]

ABSTRACT: A combination of static and dynamic laser light scattering (LLS) was used to study the "coil-to-globule" transition of poly(*N*-isopropylacrylamide) grafted with poly(ethylene oxide) (PNIPAM-*g*-PEO) in water. Two PNIPAM-*g*-PEO samples ($M_w = 7.29 \times 10^6$ and 7.85×10^5 g/mol) were prepared by free radical copolymerization of *N*-isopropylacrylamide and poly(ethylene oxide) macromonomers end-capped with methacrylate ($M_w = \sim 7000-8000$) in water. At room temperature, PNIPAM-*g*-PEO in water exists as individual chains. When the temperaturte is higher than ∼32 °C, the PNIPAM-*g*-PEO chain backbone undergoes the intrachain "coil-to-globule" transition and the interchain aggregation to form nanoparticles with a hydrophobic PNIPAM core and a soluble hydrophilic PEO shell. The nanoparticle size decreases as the average number of PEO chains grafted on the PNIPAM chain backbone increases. A lower copolymer concentration and a fast heating rate can also lead to smaller nanoparticles. With a proper control of the formation conditions, we were able to suppress the interchain aggregation to prepare and study a single chain core−shell nanostructure.

Introduction

In recent years, extensive attention has been paid to block and graft amphiphilic copolymers for their capability to form stable aggregates with a core−shell structure in solution.[1−8] For example, an amphiphilic copolymer consisting of a hydrophobic chain backbone grafted with a number of hydrophilic branches can form stable colloidal particles in water through an one-step precipitation or solvent exchange.[9] It has been shown that a very slow addition of THF or DMF solution containing individual amphiphilic copolymer chains into a large quantity of water or directly dialyzed against water can lead to stable colloidal nanoparticles with the aggregated hydrophobic backbone chains as a hydrophobic core and the soluble grafted hydrophilic branches as a hydrophilic corona shell.[10−13] The nanoparticle size is normally in the range 10−500 nm, depending on the formation conditions and the copolymer structure. Another interesting point is that such formed colloidal particles were narrowly distributed even though the copolymer chains used were polydisperse.[14,15] The formation of these novel colloidal particles presents an intriguing topic in both polymer and colloid science.

The present work is based on our previous study of the "coil-to-globule" transition of poly(*N*-isopropylacrylamide) (PNIPAM). When the temperature is lower than ∼32 °C, the PNIPAM chains are hydrophilic and exist as individual chains with a random coil conformation in water, while at higher temperatures, the PNIPAM chain backbone becomes hydrophobic and collapses into a molecular globule. Utilizing this special thermoproperty, we have prepared a set of poly(*N*-isopropylacrylamide)s grafted with different amounts of poly(ethylene oxide) chains (PNIPAM-*g*-PEO). In cold water, both the PNIPAM chain backbone and the grafted PEO branches are hydrophilic. A simple increase of temperature to ∼32 °C or higher can induce the "coil-to-globule" transition of the PNIPAM chain backbone to form stable colloidal nanoparticles with a hydrophobic PNIPAM core and a hydrophilic PEO shell. The core−shell structure can be easily switched on and off by a simple temperature variation of only 1−2 °C. Therefore, PNIPAM-*g*-PEO is a convenient model system for investigating the formation of the core−shell structure.

Experimental Section

Sample Preparation. The poly(ethylene oxide) (PEO) macromonomers end-capped with methacrylate were synthesized by anionic ring-opening polymerization of ethylene oxide (EO) in tetrahydrofuran (THF) using potassium methoxide (MeOK) as initiator.[17] EO was repeatedly purified by a trap-to-trap distillation over calcium hydride. THF was refluxed and distilled over sodium wire. Potassium methoxide was obtained by quenching potassium in cold methanol under a nitrogen atmosphere. The polymerization of a proper amount of EO and MeOK was carried out at 40 °C for 12 h. The resultant PEO potassium alkoxide was further reacted with methacryloyl chloride (MAC) for ∼1 h. The PEO macromonomers end-capped with methacrylate (PEO−MA) were finally obtained by pouring the reaction mixture into acetone. Further purification of PEO−MA was achieved by a three-cycle reprecipitation from chloroform to ether. The weight average molar mass and polydispersity of the PEO macromonomers were determined by gel permeation chromatography (GPC) using chloroform as eluent and PEO as standards. The PEO macromonomers used in this study have a weight average molar mass of 7000−8000 g/mol and a polydispersity index (M_w/M_n) of ∼1.15.

The grafting of PEO on poly(*N*-isopropylacrylamide) was done by a free-radical copolymerization of the PEO macromonomer and *N*-isopropylacrylamide (NIPAM) monomer in water at 60 °C using $K_2S_2O_8$ as initiator. NIPAM (courtesy of Kohjin Co.) was purified by recrystallization in a benzene/hexane mixture. The reaction was conducted in a 250-mL two-neck flask equipped with a nitrogen inlet tube and a magnetic stirrer. A 0.5 mmol sample of NIPAM, the proper amount of the PEO macromonomer, and 0.2 mol % of $K_2S_2O_8$ were added to 50 mL of deionized water. The total monomer concentration was kept at ∼0.5 M. After purging with nitrogen for ∼30 min, the reaction mixture was heated to 50 °C and the reaction was carried out at this temperature for 2 h in a water bath. The monomer conversion was controlled to be less than 50%. The resultant copolymer was recovered and purified. Two graft copolymers, named as PNIPAM-*g*-PEO1 and PNIPAM-*g*-PEO2, were used. PNIPAM-*g*-PEO1 with a higher molar mass was prepared in pure deionized water, while PNIPAM-*g*-PEO2 with a lower molar mass was made in an aqueous solution

[⊗] Abstract published in *Advance ACS Abstracts,* November 15, 1997.

S0024-9297(97)00894-2 CCC: $14.00

Table 1. NMR, LLS, and Differential Refractometry Characterization of the PNIPAM-*g*-PEO Copolymers

sample	M_w (g/mol)	wt % PEO	N_{PEO}	(dn/dC) (mL/g) 25 °C	(dn/dC) (mL/g) 45 °C
PNIPAM-*g*-PEO1	7.29×10^6	7.7	~70	1.61	1.63
PNIPAM-*g*-PEO2	7.85×10^5	5.9	~7	1.62	1.64

containing 1% of moderate chain transfer agent ethanol.[18] The apparent weight average molar masses (M_w) of PNIPAM-*g*-PEO1 and PNIPAM-*g*-PEO2 listed in Table 1 were determined by laser light scattering. The copolymer compositions were estimated by ^{1}H NMR. The NMR spectra were recorded in $CDCl_3$ on a Bruker DPX-300 (300 MHz) spectrometer.

Laser Light Scattering. A modified commercial LLS spectrometer (ALV/SP-125) equipped with an ALV-5000 digital time correlator and a solid-state laser (ADLAS DPY425II, output power ca. 400 mW at $\lambda = 532$ nm) was used. The incident light beam is vertically polarized with respect to the scattering plane. In static LLS, the angular dependence of the excess absolute time-averaged scattering intensity, known as the Rayleigh ratio $R_{vv}(q)$, was measured. For a dilute solution measured at a relatively small angle (θ), $R_{vv}(q)$ can be related to the weight average molar mass (M_w), the root mean square radius of gyration ($\langle R_g^2\rangle_z^{1/2}$) (or simply as $\langle R_g\rangle$), the second virial coefficient (A_2), and the scattering vector (q) as

$$\frac{KC}{R_{vv}(q)} \approx \frac{1}{M_w}\left(1 + \frac{1}{3}R_g^2 q^2\right) + 2A_2C \qquad (1)$$

where $K = 4\pi n^2(\mathrm{d}n/\mathrm{d}C)^2/(N_A\lambda_0^4)$ and $q = (4\pi n/\lambda_0)\sin(\theta/2)$ with N_A, n, dn/dC, and λ_0 being the Avogadro constant, the solvent refractive index, the specific refractive index increment, and the wavelength of light in vacuum, respectively. The values of dn/dC were calculated using the additive equation:[19]

$$\mathrm{d}n/\mathrm{d}C = W_{PEO}(\mathrm{d}n/\mathrm{d}C)_{PEO} + W_{PNIPAM}(\mathrm{d}n/\mathrm{d}C)_{PNIPAM} \qquad (2)$$

where W represents the weight fraction. All the solutions and dispersions were clarified using 0.5-μm or 0.1-μm Millipore filters depending on the size of the particles, so that dust was removed, but not the polymer chains.

In dynamic LLS, the intensity−intensity time correlation function $G^{(2)}(t,\theta)$ in the self-beating mode was measured. $G^{(2)}(t,\theta)$ is related to the normalized first-order electric field time correlation function $g^{(1)}(t,\theta)$ as[20]

$$G^{(2)}(t,\theta) = \langle I(0,\theta)\, I(t,\theta)\rangle = A[1 + \beta|g^{(1)}(t,\theta)|^2] \qquad (3)$$

where A is the measured base line, β is a parameter depending on the coherence of the detection, and t is the delay time. For a polydisperse sample, $g^{(1)}(t,\theta)$ is related to the line-width distribution G(Γ) by

$$g^{(1)}(t,\theta) = \langle E(t,\theta)\, E^*(0,\theta)\rangle = \int_0^\infty G(\Gamma)\mathrm{e}^{-\Gamma t}\,\mathrm{d}\Gamma \qquad (4)$$

Using a Laplace inversion program, CONTIN, in the correlator, we were able to calculate $G(\Gamma)$ from $G^{(2)}(t,\theta)$ on the basis of eqs 3 and 4. For a pure diffusive relaxation, $\Gamma = D/q^2$ if the solution is dilute and $qR_g \ll 1$, where D is the translational diffusive coefficient. D can be further converted into the hydrodynamic radius R_h using the Stokes−Einstein equation: $D = k_BT/6\pi\eta R_h$, where k_B, T, and η are the Boltzmann constant, the absolute temperature, and the solvent viscosity, respectively. All the dynamic light scattering experiments were done at $\theta = 15°$ except otherwise stated.

Results and Discussion

Figure 1 shows a typical ^{1}H-NMR spectrum of PNIPAM-*g*-PEO. The assignment of each proton shows that the ^{1}H-NMR spectrum is consistent with the expected copolymer structure depicted in Figure 1. The typical resonance of the methylene protons of PEO appears at 3.64 ppm, indicating a successful grafting of the PEO macromonomer to the PNIPAM chain backbone. The peak at 1.20 ppm can be attributed to the methyl protons of the *N*-isopropyl group. The resonances at 2.26 and 2.17 ppm are respectively assigned to the methylene protons of the PNIPAM chain backbone. The signal at 4.00 ppm is assigned to the methylene protons of the *N*-isopropyl group. By taking the area ratio of the PEO protons to the PNIPAM protons, we were able to estimate the weight percentage of PEO (PEO wt %) in the copolymer and the average number (N_{PEO}) of grafted PEO chains on each PNIPAM chain backbone. The NMR results are also listed in Table 1. On average, each PNIPAM-*g*-PEO1 chain has ~10 times more grafted PEO branches than PNIPAM-*g*-PEO2, but the two copolymers have a similar average length of the PNIPAM segment between the two neighboring grafted PEO branches.

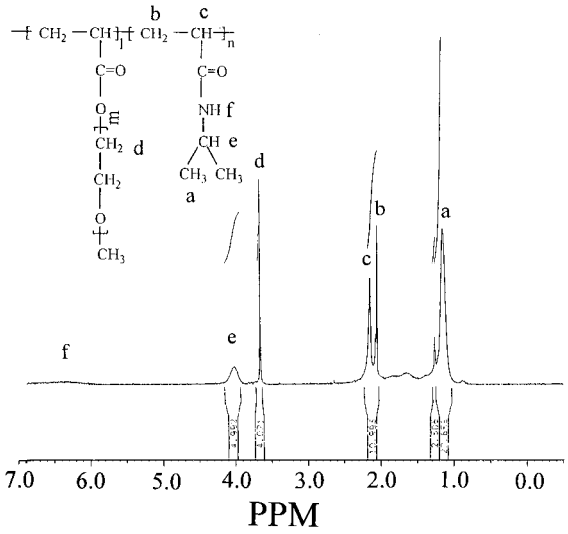

Figure 1. Typical ^{1} NMR spectrum of PNIPAM-*g*-PEO1 in $CDCl_3$ at 25 °C.

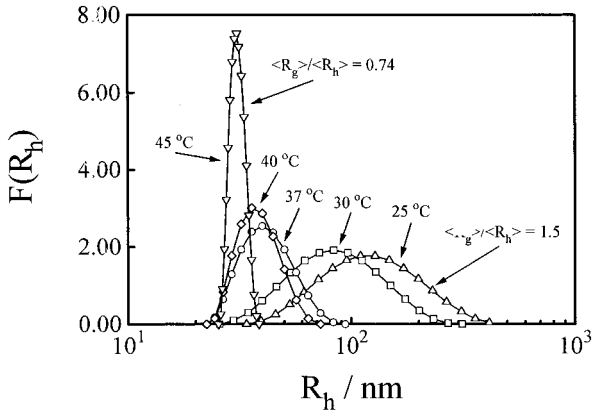

Figure 2. Temperature dependence of the hydrodynamic radius distribution ($f(R_h)$) of PNIPAM-*g*-PEO1 in deionized water, where $C = 1 \times 10^{-4}$ g/mL.

Figure 2 shows a typical plot of the temperature dependence of the hydrodynamic radius distribution ($f(R_h)$) of PNIPAM-*g*-PEO1, where $C = 1.00 \times 10^{-4}$ g/mL. It shows that as the temperature increases, the distribution shifts to the left (i.e., the hydrodynamic radius decreases) and the distribution becomes narrower, similar to the results observed in other systems.[14,15] Another important point is that the ratio of the radius of gyration to the hydrodynamic radius ($\langle R_g\rangle/\langle R_h\rangle$) decreases from a value of 1.5, predicted for a

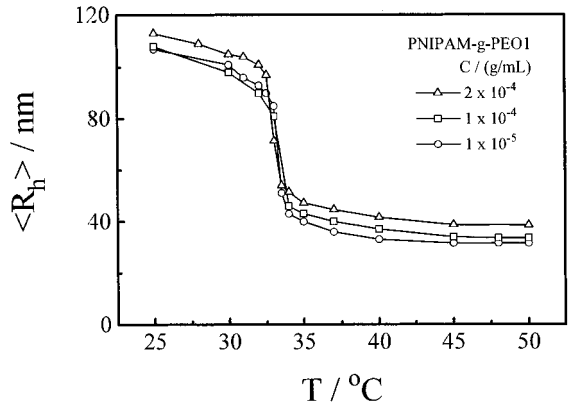

Figure 3. Temperature and concentration dependence of the average hydrodynamic radius $\langle R_h \rangle$ of PNIPAM-*g*-PEO1 in deionized water.

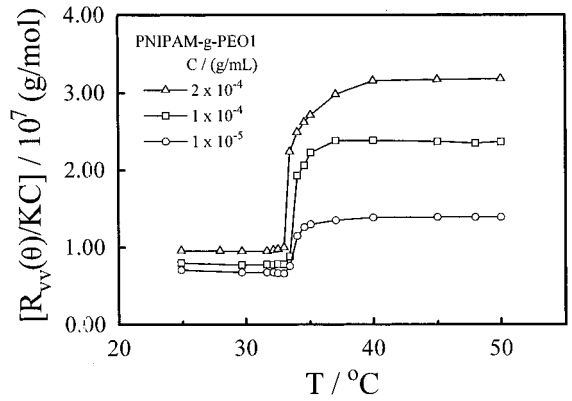

Figure 4. Temperature and concentration dependence of the excess scattering intensity $R_{vv}(\theta)/KC$ of PNIPAM-*g*-PEO1 in deionized water.

random-coil chain in a good solvent, to 0.74, close to 0.774 for a uniform sphere. The decrease of $\langle R_g \rangle/\langle R_h \rangle$ clearly indicates the collapse of the copolymer chains from a random coil to a globule.

Figures 3 and 4, respectively, show the temperature and concentration dependence of the average hydrodynamic radius $\langle R_h \rangle$ and the excess scattering intensity $R_{vv}(\theta)/KC$ of PNIPAM-*g*-PEO1 in water, where $\langle R_h \rangle$ was calculated from $f(R_h)$ shown in Figure 2 on the basis of $\langle R_h \rangle = \int_0^\infty R_h f(R_h)\, dR_h$ and $R_{vv}(\theta)/KC$ is proportional to the weight average molar mass M_w on the basis of eq 1. Here, the increase of temperature from 25 to 50 °C was slow and step by step; i.e., it was stopped at each measurement temperature and the LLS measurement at each temperature was conducted after the equilibrium was reached.

The change of $\langle R_h \rangle$ can be divided into three stages: (1) when the temperature increases from 25 to 32 °C, water progressively becomes a poor solvent for the PNIPAM chain backbone, resulting in a slight decrease of $\langle R_h \rangle$; (2) in the range ~32−34 °C, the PNIPAM chain backbone undergoes the intrachain "coil-to-globule" transition so that $\langle R_h \rangle$ rapidly decreases; and (3) at temperatures higher than ~34 °C, the PNIPAM chain backbone is already in its fully collapsed state so that a further increase of temperature has little effect on $\langle R_h \rangle$.

On the other hand, as shown in Figure 4, when the temperature is lower than ~32 °C, $R_{vv}(\theta)/KC$ is nearly independent of temperature with a value in the range $(7-8) \times 10^6$ g/mol, very close to the weight average molar mass of individual PNIPAM-*g*-PEO1 chains,

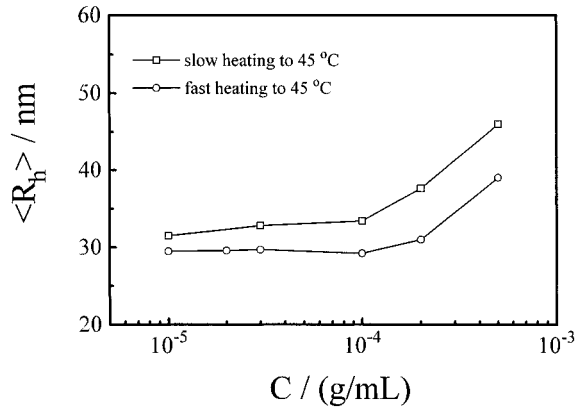

Figure 5. Heating-rate dependence of the average hydrodynamic radius $\langle R_h \rangle$ of PNIPAM-*g*-PEO1 in deionized water, where "the slow heating" means a step-by-step increase of temperature from 25 to 45 °C, while "the fast heating" means a one-step temperature jump from 25 to 45 °C.

indicating no interchain aggregation. This is expected since both the PNIPAM chain backbone and PEO branches are hydrophilic and soluble in water in this temperature range. An abrupt increase of $R_{vv}(\theta)/KC$ at ~33 °C clearly indicates the interchain aggregation. Over a narrow temperature range of ~33−36 °C, each $R_{vv}(\theta)/KC$ curve reaches a higher plateau, implying the formation of stable nanoparticles. From the value of each higher plateau and the average molar mass of individual PNIPAM-*g*-PEO1 chains, we are able to estimate the average number of copolymer chains ($N_{\text{PNIPAM-}g\text{-PEO}}$) inside each nanoparticle. In Figure 4, $N_{\text{PNIPAM-}g\text{-PEO}}$ has a value of ~2, ~3, and ~4, respectively.

A comparison of Figures 3 and 4 reveals that the formation of the PNIPAM-*g*-PEO nanoparticles actually involves two simultaneous processes: the intrachain "coil-to-globule" transition and the interchain aggregation. The number of the grafted PEO chains in each particle linearly increases as the number of the PNIPAM-*g*-PEO chains inside the particle increases, or in other words, it increases as the particle mass (M_{particle}) increases, while the particle surface area is only proportional to R^2, i.e., $M_{\text{particle}}^{2/3}$. Therefore, the surface area per grafted PEO chain decreases as the aggregation proceeds until the nanoparticles are stabilized by a sufficient amount of the PEO chains on the nanoparticle surface. The shrinking of the PNIPAM chain backbone also decreases the surface area per PEO chain and helps to prevent further aggregation. At higher copolymer concentrations, individual copolymer chains have more chance to aggregate with each other before they are collapsed and stabilized by the grafted PEO chains. This is why the size of the nanoparticles increases as the copolymer concentration increases. It is logic to expect that by reducing the copolymer concentration we will be able to suppress the interchain aggregation to obtain individual single chain core−shell nanoparticles.

Figure 5 shows the heating rate dependence of $\langle R_h \rangle$ for PNIPAM-*g*-PEO1 in water, where "the slow heating" represents the step-by-step increase of temperature from 25 to 45 °C, while "the fast heating" means a one-step temperature jump from 25 to 45 °C. It shows that for a given copolymer concentration the nanoparticles formed by means of the slow heating is systematically larger than that formed in the fast heating process. This can also be attributed to the competition between the

Table 2. Laser Light Scattering Characterization of the PNIPAM-*g*-PEO1 Core−Shell Nanoparticles in Deionized Water at 25 °C

C (g/mL)	heating rate	$M_{particle}$ (g/mol)	$\langle R_h \rangle$ (nm)	$N_{PNIPAM\text{-}g\text{-}PEO}$	N_{PEO}	$\langle \rho \rangle_{particle}$ (g/cm^3)	$\langle R \rangle_{core}$ (nm)	$\langle \rho \rangle_{core}$ (g/cm^3)	S_{PEO} (nm^2)
5×10^{-4}	slow	6.15×10^7	45.5	8.4	592	0.259	39.5	0.365	33.1
2×10^{-4}	slow	3.20×10^7	38.0	4.4	308	0.231	32.0	0.358	41.8
1×10^{-4}	slow	2.32×10^7	34.9	3.2	223	0.217	28.9	0.352	47.0
1×10^{-5}	slow	1.45×10^7	30.8	2.0	140	0.196	24.8	0.348	55.2
5×10^{-4}	fast	3.48×10^7	39.1	4.7	329	0.229	33.1	0.354	41.8
1×10^{-4}	fast	1.15×10^7	29.2	1.5	105	0.182	23.2	0.337	64.3
1×10^{-5}	fast	7.95×10^6	29.0	1.0	77	0.129	23.0	0.240	86.3

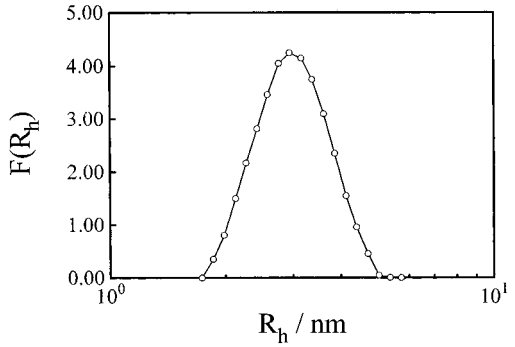

Figure 6. Hydrodynamic radius distribution $f(R_h)$ of the PEO macromonomer chains free in deionized water at 45 °C.

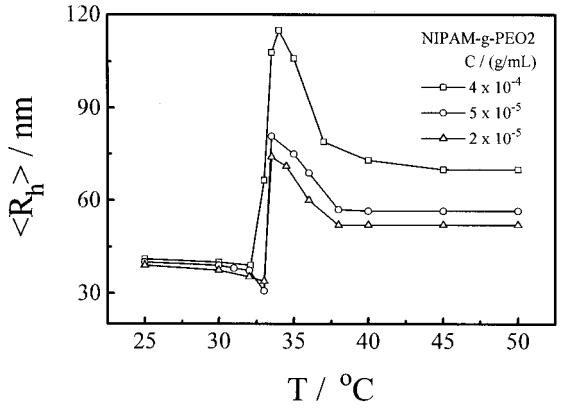

Figure 7. Temperature and concentration dependence of the average hydrodynamic radius $\langle R_h \rangle$ of PNIPAM-*g*-PEO2 in deionized water.

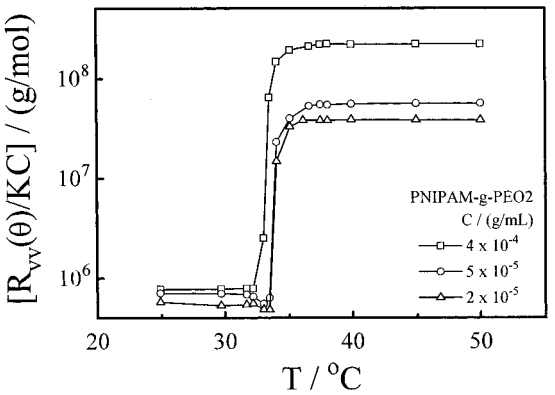

Figure 8. Temperature and concentration dependence of the excess scattering intensity $R_{vv}(\theta)/KC$ of PNIPAM-*g*-PEO2 in deionized water.

intrachain "coil-to-globule" transition and the interchain aggregation. In the fast heating process, individual copolymer chains have less chance to aggregate with each other before they are collapsed into individual globules and stabilized by the grafted PEO chains. It was worth noting that in the fast heating process $\langle R_h \rangle$ is independent of C as long as C is lower than 1×10^{-4} g/mL. The static LLS results (not shown) also reveal that in the same concentration range the nanoparticles and individual copolymer chains have a very similar weight average molar mass, indicating that by means of the fast heating each nanoparticle formed in a dilute solution contains only one copolymer chain. We have successfully made a single chain core−shell nanostructure.

Table 2 summarizes the characterization of the PNIPAM-*g*-PEO1 nanoparticles formed under different conditions. The overall apparent average chain density ($\langle \rho \rangle_{particle}$) was estimated on the basis of $\langle \rho \rangle_{particle} = M_{w,particle}/(4/3\pi \langle R_h \rangle^3 N_A)$, with N_A being the Avogadro constant. The values of $\langle \rho \rangle_{particle}$ are considerably lower than the value (~0.35 g/cm^3) of the collapsed PNIPAM homopolymer chains,[21] which can be reasonably attributed to the existence of the low-density soluble PEO shell. It is known that the average hydrodynamic radius of the PEO macromonomer chains free in water at 45 °C is ~3 nm (shown in Figure 6). Assuming that the PEO chains grafted on the nanoparticles behave the same as the PEO chains free in water, we can reasonably estimate the thickness of the PEO shell (L_{shell}) to be ~6 nm and the radius of the core ($\langle R \rangle_{core}$) from the difference between $\langle R_h \rangle$ and L_{shell}. Further, we can respectively estimate the average density of the core ($\langle \rho \rangle_{core}$) from the total mass of the PNIPAM chain backbones inside the core and the surface area per PEO chain (S_{PEO}) from the average number of the grafted PEO chains per nanoparticle. The values of $\langle R \rangle_{core}$, $\langle \rho \rangle_{core}$, and S_{PEO} are also summarized in Table 2.

It is worth noting the S_{PEO} decreases and approaches the cross section (~30 nm^2) of the PEO chain as $N_{PNIPAM\text{-}g\text{-}PEO}$ increases. This shows that the PEO chains grafted on a multichain nanoparticle are not overlapped on the particle surface. On the other hand, for the nanoparticle containing only 1−2 copolymer chains, the large values of S_{PEO} indicate the average distance between the two neighboring PEO chains is even larger than the size of the PEO chains; i.e., the PEO chains are separated from each other on the particle surface. Therefore, it is reasonable to assume that the PEO chains grafted on the surface and free in water have a similar conformation; i.e., the PEO chains grafted on the surface can be viewed as individual "mushrooms".[21] When $N_{PNIPAM\text{-}g\text{-}PEO} > 2$, $\langle \rho \rangle_{core}$ is nearly a constant, similar to the previous results.[22] It is interesting to note that $\langle \rho \rangle_{core}$ drops when the nanoparticle is made of only a single PNIPAM-*g*-PEO chain. This lower core density can be attributed to the fact that the approaching of two *intrachain* segments is relatively more difficult than that of two *interchain* segments, so that the packing of the chain segments inside a single chain nanoparticle is relatively loose.[23]

Figures 7 and 8, respectively, show the temperature and concentration dependence of the average hydrodynamic radius $\langle R_h \rangle$ and the excess scattering intensity $R_{vv}(\theta)/KC$ of short PNIPAM-*g*-PEO2 chains in water. Figure 7 reveals that short chains follow a different

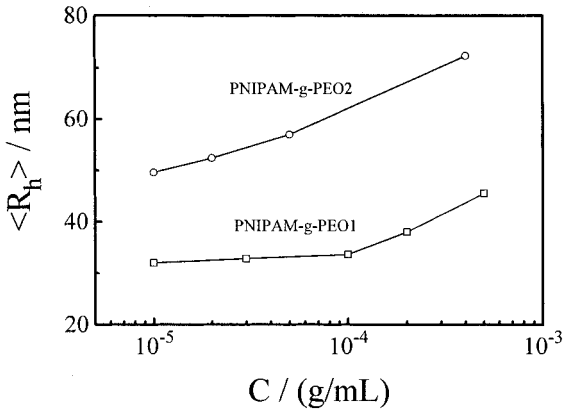

Figure 9. Comparison of the average hydrodynamic radius $\langle R_h \rangle$ of the PNIPAM-*g*-PEO1 and PNIPAM-*g*-PEO2 nanoparticles formed with different initial polymer concentrations in the step-by-step slow heating from 25 to 45 °C.

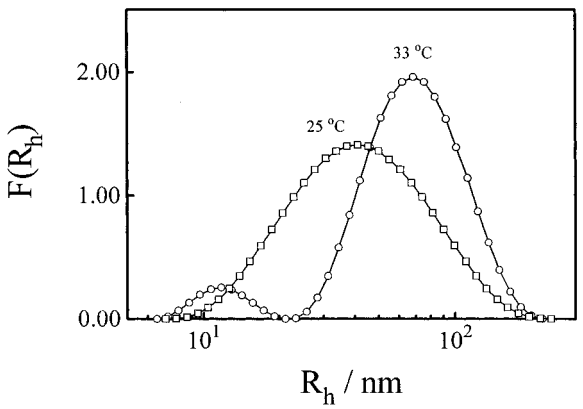

Figure 10. Hydrodynamic radius distribution ($f\langle R_h \rangle$) of PNIPAM-*g*-PEO2 in deionized water at two different temperatures, where $C = 4 \times 10^{-4}$ g/mL.

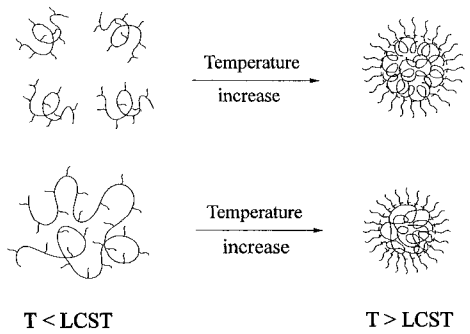

Figure 11. Schematic of two different nanoparticle formation mechanisms respectively related to short and long PNIPAM-*g*-PEO chains.

nanoparticle formation process; namely, after reaching a maximum at ~33.5 °C, $\langle R_h \rangle$ starts to decrease, while in the case of long PNIPAM-*g*-PEO1 chains (Figure 3) $\langle R_h \rangle$ remains constant after reaching the maximum value. However, there is no difference in the changing pattern of $R_{vv}(\theta)/KC$ between long and short chains (Figure 4 and 8). Therefore, the decrease of $\langle R_h \rangle$ in Figure 7 and the constant values of $R_{vv}(\theta)/KC$ in Figure 8 lead to only one possibility; i.e., for short PNIPAM-*g*-PEO2 chains, the interchain aggregation is prior to the intrachain "coil-to-globule" transition. The average aggregation numbers of short chains inside each PNIPAM-*g*-PEO2 nanoparticle are ~80, ~90, and ~280, respectively, for $C = 2 \times 10^{-5}$, 5×10^{-5}, and 4×10^{-4} g/mL, which also reflect that the interchain aggregation is dominant in the case of short chains.

Figure 9 shows a comparison of the nanoparticles respectively made of PNIPAM-*g*-PEO1 and PNIPAM-*g*-PEO2 after the step-by-step slow heating from 25 to 45 °C. For a given copolymer concentration, the nanoparticles made of PNIPAM-*g*-PEO2 are systematically larger than that made of PNIPAM-*g*-PEO1. The larger size of the PNIPAM-*g*-PEO2 nanoparticles further indicates that the interchain aggregation is dominant when short chains were used. This is understandable because, on average, each PNIPAM-*g*-PEO1 chain has ~10 times more grafted PEO macromonomer chains so that the stabilization of the PNIPAM-*g*-PEO1 nanoparticles can be reached when the aggregates are relatively small.

Figure 10 shows a better view of the competition between the intrachain "coil-to-globule" transition and the interchain aggregation in terms of the change of the hydrodynamic radius distribution ($f\langle R_h \rangle$) of PNIPAM-*g*-PEO2 at two different temperatures, where $C = 4 \times 10^{-4}$ g/mL. At 33 °C, the initial monomode distribution is split into a bimode distribution. The peak located at ~80 nm can be attributed to the interchain aggregates, while the peak located at ~15 nm reflects individual collapsed copolymer chains. Figure 11 schematically shows two formation processes respectively related to the short and long PNIPAM-*g*-PEO chains.

Conclusion

The formation of the PNIPAM-*g*-PEO nanoparticles with a "core−shell" structure involves two processes: the intrachain "coil-to-globule" transition and the interchain aggregation. For the short PNIPAM-*g*-PEO chains, the interchain aggregation is dominant. On the one hand, for a given copolymer concentration, the fast heating can suppress the interchain aggregation; and on the other hand, for a given heating rate, diluting the copolymer solution can also suppress the interchain aggregation. Using longer copolymer chains, a dilute solution, and a fast temperature jump, we have successfully made a single chain particle with a "core−shell" nanostructure.

Acknowledgment. The financial support of the Research Grants Council of Hong Kong Government Earmarked Grant 1995/96 (CUHK 305/96P, 2160063) is gratefully acknowledged. X.Q. is grateful to the Chinese University of Hong Kong for awarding him an one-year postdoctoral fellowship.

References and Notes

(1) Gao, Z.; Varshney, S. K.; Wong, S.; Eisenberg, A. *Macromolecules* **1994**, *27*, 7923.
(2) Zhang, L.; Shen, H.; Eisenberg, A. *Macromolecules* **1997**, *30*, 1001.
(3) Antonietti, M.; Heinz, S.; Schmidt, M.; Rosenauer, C. *Macromolecules* **1994**, *27*, 3276.
(4) Henselwood, F.; Liu, G. *Macromolecules* **1997**, *30*, 488.
(5) Qiu, Y.; Yu, X.; Feng, L.; Yang, S. *Chin. J. Polym. Sci.* **1993**, *11*, 67.
(6) Berlinova, I. V.; Amzil, A.; Tsvetkova, S.; Panayotov, I. M. *J. Polym. Sci., Polym. Chem.* **1994**, *32*, 1523.
(7) Gao, B.; Wesslen, B.; Wesslen, K. B. *J. Polym. Sci., Polym. Chem.* **1992**, *30*, 1799.
(8) Wesslen, B.; Derand, H. *J. Polym. Sci., Polym. Chem.* **1995**, *33*, 571.
(9) Barany, G.; Zalipsky, S.; Chang, J. L.; Albericio, F. *React. Polym.* **1994**, *22*, 243.
(10) Selb, J.; Gallot, Y. *Makromol. Chem.* **1980**, *181*, 809; *182*, 1491.
(11) Li, M.; Zhu, L.; Jiang, M.; Wu, C. *Macromolecules* **1997**, *30*, 2201−2203.

(12) Gref, R.; Minamitake, Y.; Peracchia, M. T.; Trubetskoy, V.; Torchilin, V.; Langer, R. *Science* **1994**, *263*, 1600.
(13) Fessi, H.; Puisieux, F.; Devissaguet, J. Ph.; Ammoury, N.; Benita, S. *Int. J. Pharm.* **1989**, *55*, R1.
(14) Eckert, A. R.; Webber, S. E. *Macromolecules* **1996**, *29*, 560.
(15) Peracchia, M. T.; Desmaele, D.; Couvreur, P.; d'Angelo, J. *Macromolecules* **1997**, *30*, 846.
(16) Wu, C.; Zhou, S. *Macromolecules* **1995**, *28*, 8381.
(17) Ito, K.; Tsuchida, H.; Hayashi, A.; Kitano, T.; Yamada, E.; Matsumoto, T. *Polym. J.* **1985**, *17* (7), 827.
(18) Qiu, X.; Wu, C. *Macromolecules*, submitted for publication.
(19) Zhou, Z.; Chu, B.; Peiffer, D. G. *Macromolecules* **1993**, *26*, 1876.
(20) Chu, B. *Laser Light Scattering*, 2nd ed.; Academic Press: New York, 1991.
(21) Kawaguchi, S.; Winnik, M. A.; Ito, K. *Macromolecules* **1995**, *28*, 1159.
(22) Qiu, X.; Kwan, C. M. S.; Wu, C. *Macromolecules*, submitted for publication.
(23) Wu, C.; Chan, K. K.; Woo, K. F.; Qian, R. Y.; Liu, X.; Chen, L.; Napper, D. H.; Tan, G.; Hill, A. J. *Macromolecules* **1995**, *28*, 1592.

MA970894G